Terahertz-wave parametric gain of stimulated polariton scattering

Yuma Takida,[1,*] Jun-ichi Shikata,[2] Kouji Nawata,[1] Yu Tokizane,[1] Zhengli Han,[1] Mio Koyama,[1] Takashi Notake,[1] Shin'ichiro Hayashi,[1] and Hiroaki Minamide[1]

[1]*Tera-Photonics Research Team, RIKEN Center for Advanced Photonics (RAP), RIKEN, Sendai 980-0845, Japan*

[2]*College of Engineering, Nihon University, Koriyama 963-8642, Japan*

(Received 5 November 2015; revised manuscript received 24 February 2016; published 21 April 2016)

We have experimentally determined the terahertz- (THz-) wave parametric gain of stimulated Raman scattering (SRS) by phonon-polaritons in $LiNbO_3$. Our approach is based on ultrabright THz-wave generation from SRS under stimulated Brillouin scattering suppression with subnanosecond pump pulses. To obtain the frequency dependence of the parametric gain, we measured the crystal-length dependence of the THz-wave output directly using a surface-coupling configuration. We found that the product of the parametric gain and the threshold crystal length is constant throughout the tuning range. Our result provides a physical basis for the design and performance enhancement of SRS-based ultrabright tabletop THz-wave sources for various applications.

DOI: 10.1103/PhysRevA.93.043836

Recent progress in the generation of intense terahertz- (THz-) wave pulses has opened the door to new fields of fundamental science and practical applications [1]. In particular, narrowband and frequency-tunable THz-wave pulses are highly important for the resonant excitation and coherent control of low-energy light-matter interactions, such as radiation-enhanced superconductivity [2], excitation of the Higgs mode in superconductors [3], excitation of intraexcitonic transition in quantum systems [4], and manipulation of magnetic ordering in multiferroic materials [5]. Until now, these experiments have been reliant on large-scale far-infrared free-electron laser facilities or complex high-energy femtosecond laser-based systems. In addition to these sources, ultrabright continuously tunable multicycle THz-wave sources driven by a compact and simple laser setup may facilitate the study of unexplored resonantly induced nonlinear phenomena in a variety of research fields.

Since the late 1960s, phonon-polaritons, which result from strong coupling between photons and optical phonons in nonlinear crystals, have been attracting considerable interest with regard to the generation of coherent THz-wave radiation [6–13]. A recent experimental study on $LiNbO_3$ has shown that the conversion efficiency of THz-wave generation via stimulated Raman scattering (SRS) by phonon-polaritons can be improved by three orders of magnitude through the use of subnanosecond (subns) pump pulses [14]. Such short-time pulses provide a pump intensity on the order of GW/cm^2 for SRS without stimulated Brillouin scattering (SBS) because the subns pulse duration is shorter than the steady-state SBS buildup time in $LiNbO_3$ [15,16]. For this pump condition, the frequency dependence of the THz-wave output from the SRS becomes almost flat in the wide frequency range of $1-3$ THz [14]. This result means that the exponent $g_{\mathrm{THz}}L$ is frequency independent, where g_{THz} is the THz-wave parametric gain of SRS by phonon-polaritons and L is the crystal length. However, the individual frequency dependencies of g_{THz} and L experimentally are determined here. This is because accurate measurement of the L dependence of the THz-wave output is hampered by the strong absorption of the crystal itself [17], the noncollinear phase-matching condition of the SRS [18], and the necessity of employing crystals with different L's.

The frequency dependence of g_{THz} has been predicted theoretically using phonon-polariton damping models [19,20]. Under constant damping, g_{THz} exhibits a smooth frequency dependence [19]. Ushioda *et al.* have reported the temperature dependence of a constant damping function at $345\,\mathrm{cm}^{-1}$ in GaP measured using spontaneous Raman scattering [21]. On the other hand, with regard to frequency-dependent damping including low-frequency modes, g_{THz} has a frequency dependence with a dip structure [20]. Schwarz and Maier have reported the frequency-dependent Raman gain for Stokes waves (referred to as "idler" waves in this paper) in $LiNbO_3$ measured using SRS [22,23]. In that experiment, however, the frequency dependence of the SRS gain was affected by low-frequency modes excited in the SBS because the 10-ns pump pulse was significantly longer than the steady-state SBS buildup time in $LiNbO_3$. Therefore, a comparison between the theoretically predicted and the experimentally measured frequency dependence of g_{THz} under SBS suppression is essential, particularly with regard to the design and performance enhancement of SRS-based ultrabright tabletop THz-wave sources.

In this paper, we report an accurate measurement of g_{THz} in $LiNbO_3$. Our approach is based on ultrabright THz-wave generation from SRS under SBS suppression using subns pump pulses. To obtain the frequency dependence of g_{THz}, we measure the L dependence of the THz-wave output directly using a surface-coupling configuration. As a result, we successfully determine the frequency dependence of g_{THz} and find that the product of g_{THz} and the threshold crystal length L_{th} of the THz-wave output is constant throughout the tuning range. Our result provides a physical basis for the design of ultrabright THz-wave sources based on the SRS by phonon-polaritons.

To measure the L dependence of the THz-wave output from the SRS by phonon-polaritons, we here propose the use of a surface-coupling configuration based on a trapezoidal $LiNbO_3$ crystal [24]. A schematic of the experimental setup is shown in Fig. 1. In this configuration, the surface of the trapezoidal crystal is used for THz-wave coupling. On the other hand, both the pump and the idler waves experience

*Corresponding author: yuma.takida@riken.jp

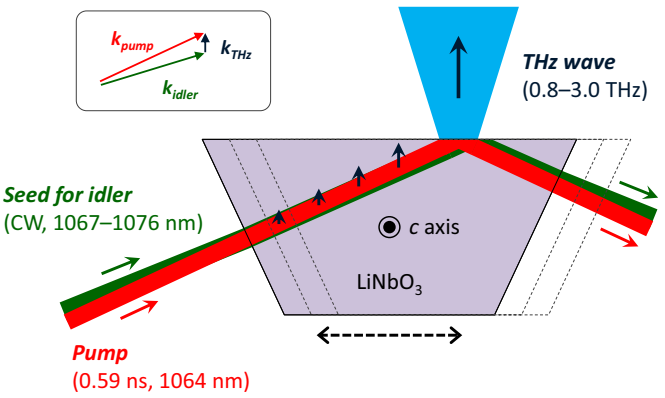

FIG. 1. Schematic of the experimental setup for gain measurement. The crystal length is continuously variable through translation of the crystal position as indicated by the dashed arrow. The inset shows the noncollinear phase-matching condition.

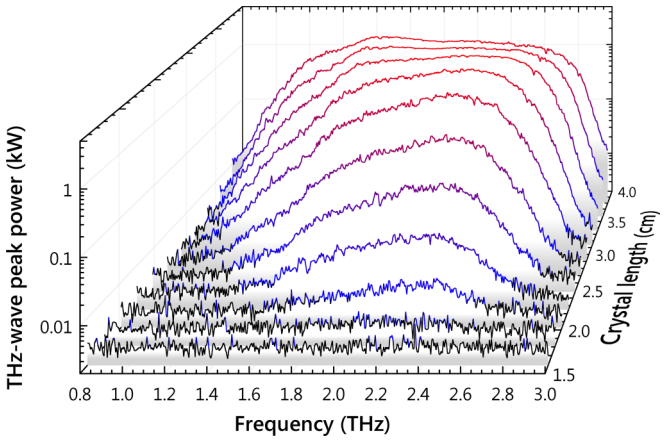

FIG. 2. Measured THz-wave peak power as a function of frequency and crystal length at 1.25-GW/cm^2 pump intensity.

total internal reflection at this surface. Consequently, this configuration has two important advantages with regard to measuring the L dependence of the THz-wave output: The THz-wave absorption loss near the coupling surface can be minimized because the propagation distance of the THz wave inside the crystal is close to zero, and the effective L, which is defined by the distance between the pump-incident and the total-reflection positions, is continuously variable via translation of the crystal as indicated by the dashed arrow in Fig. 1. Therefore, this configuration enables us to measure the L dependence of the THz-wave output without changing the crystal size. In this experiment, we used a 5-mol % MgO-doped congruent $LiNbO_3$ crystal with a bottom length of 45 mm, a height of 21 mm, and a base angle of 65.7°.

To suppress the SBS, the $LiNbO_3$ crystal was pumped by 0.59-ns pulses from a microchip Nd:YAG laser (L11038-01, Hamamatsu Photonics K. K.) with a wavelength of 1064 nm and a repetition rate of 30 Hz. The pump-wave pulse energy was amplified up to 15 mJ/pulse by a Nd:YAG amplifier. A continuous-wave (cw) output of 500 mW from an external cavity diode laser (ECDL) (λ-Master 1040, Spectra Quest Lab., Inc.) and a Yb-fiber amplifier was used for injection seed for the idler wave. The pump- and seed-beam diameters at the crystal were set to 1.47 and 1.69 mm, respectively, at full width at half maximum. In our experiment, the pump intensity was fixed at 1.25 GW/cm^2. To satisfy the SRS noncollinear phase-matching condition without adjusting the optical arrangement, an achromatic phase-matching geometry consisting of a grating and confocal telescope was applied [25]. By changing the ECDL wavelength from 1067 to 1076 nm, the THz-wave frequency could be continuously tuned from 0.8 to 3.0 THz. The THz wave emitted from the crystal was measured using a pyroelectric detector, and the THz-wave optical paths were purged with dry N_2 gas to prevent absorption loss due to water vapor. The polarization directions of all the waves were parallel to the c axis of $LiNbO_3$.

To measure the L dependence of the THz-wave output, L was varied in the 1.6−3.8-cm range. Figure 2 shows the measured THz-wave peak power as a function of frequency and L. Note that thresholdlike behavior was observed with the value of L_{th} depending on the THz-wave frequency. For $L > L_{th}$, the THz-wave output increased exponentially and then became saturated; this was primarily due to pump depletion and cascade processes [26]. At $L = 3.8$ cm, the peak power of the THz waves was measured to be more than 1 kW for a wide frequency range of 1.3−2.7 THz. This flat output profile means that g_{THz} has smooth frequency dependence; this is similar to the theoretical prediction based on the phonon-polariton constant damping model.

To obtain the frequency dependencies of g_{THz} and L_{th}, the measured L dependence of the THz-wave output was examined at each frequency. Figure 3 shows typical examples at 1.0, 1.6, 2.3, and 2.8 THz. From these data, the slope efficiencies and L_{th} were determined as shown by the dashed lines and solid arrows, respectively. These slope efficiencies correspond exactly to g_{THz} because the THz-wave output was measured directly as a function of L. In our analysis,

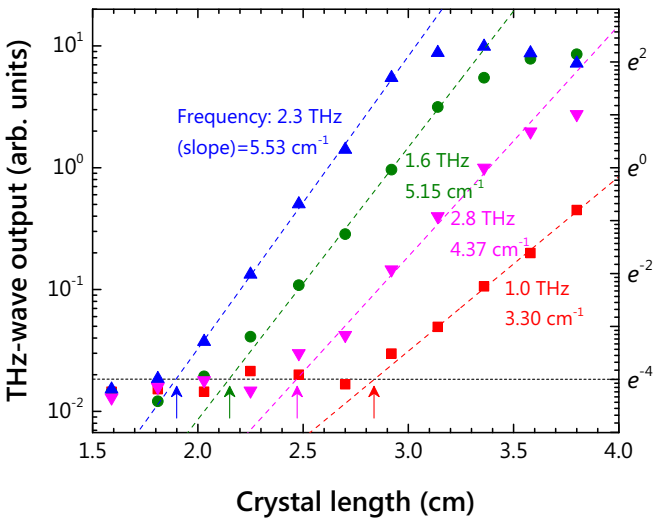

FIG. 3. Crystal-length dependence of THz-wave output. The squares, circles, triangles, and inverted triangles represent the experimental data obtained at 1.0, 1.6, 2.3, and 2.8 THz, respectively. The dashed lines represent the best fit for these data, and the slope efficiencies correspond to the gain coefficient g_{THz}. The solid arrows indicate the threshold crystal length L_{th}. The dotted horizontal line shows the noise level of the pyroelectric detector.

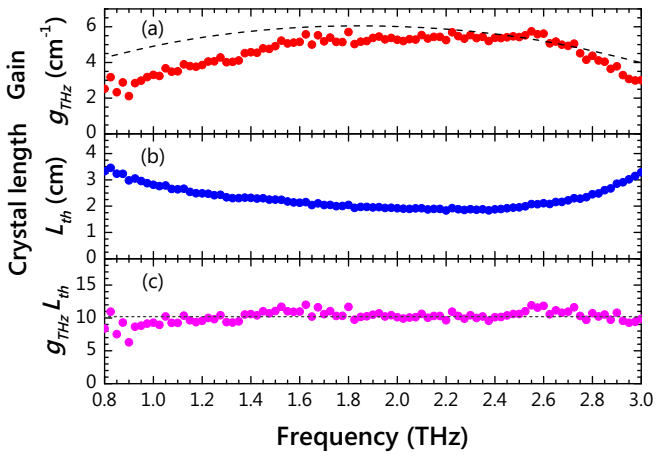

FIG. 4. Frequency dependencies of: (a) parametric gain g_{THz}, (b) threshold crystal length L_{th}, and (c) product of g_{THz} and L_{th} at 1.25-GW/cm^2 pump intensity. The dashed curve in (a) shows the calculated gain profile based on the constant damping model incorporating the propagation of the THz wave outside the interaction volume. The horizontal dotted line in (c) indicates the constant value of 10.

each L_{th} was defined as the point of intersection between the corresponding slope-efficiency fitted line (dashed lines, Fig. 3) and the noise level of the pyroelectric detector (horizontal dotted line, Fig. 3).

Figures 4(a) and 4(b) show the frequency dependencies of g_{THz} and L_{th}, respectively. The measured g_{THz} exhibits a smooth frequency dependence with a maximum at approximately 2.4 THz. On the other hand, L_{th} reaches a minimum at approximately the same frequency. This means that L_{th} is inversely proportional to g_{THz}, and the product of g_{THz} and L_{th} is frequency independent. To confirm this relationship, we calculated the product of g_{THz} and L_{th}, the result of which is shown in Fig. 4(c). Hence, we found that $g_{\mathrm{THz}}L_{\mathrm{th}}$ is constant throughout the tuning range with a value of approximately 10. Note that the constant character of $g_{\mathrm{THz}}L_{\mathrm{th}}$ is independent of the definition of L_{th}.

To compare our experimental result with the theoretical prediction, we calculated the frequency dependence of g_{THz} using the phonon-polariton constant damping model because no dip structure resulting from frequency-dependent damping was observed. According to the plane-wave approach [19,20], g_{THz} is given by

$$g_{\mathrm{THz}} = \frac{(\alpha + \alpha_{pr})}{2}\left[\sqrt{1 + 16\,\cos\varphi\left(\frac{g_0}{\alpha + \alpha_{pr}}\right)^2} - 1\right], \quad (1)$$

where α is the absorption coefficient of $LiNbO_3$ for the THz wave, α_{pr} is the additional loss factor described below, φ is the phase-matching angle between the pump and the THz waves, and g_0 is the parametric gain in the low-loss limit. Furthermore, g_0 is expressed as

$$g_0 = \sqrt{\frac{\pi\omega_{\mathrm{THz}}\omega_i I_P}{2c^3 n_{\mathrm{THz}} n_i n_p}}\,\chi_P. \quad (2)$$

In this expression, the subscripts $j = p,i$, and THz refer to the pump, the idler, and the THz waves, respectively, ω_j is the frequency, I_P is the pump intensity, c is the speed of light, n_j is the refractive index, and χ_P is the effective $\chi^{(2)}$, including electronic and ionic contributions.

To calculate g_{THz}, the following two noncollinear interactions were considered: overlapping between the pump and the idler waves and propagation of the THz wave outside the interaction volume. With regard to the former because the noncollinear phase-matching angle between the pump and the idler waves is smaller than 1.4°, the overlapping factor of these two Gaussian beams was calculated to be more than 80% throughout the tuning range. Then, the additional loss factor was estimated to be less than 0.1 cm^{-1}, which is considerably smaller than the absorption coefficient of the crystal itself. Thus, we neglected this factor in the calculation. The second factor, i.e., the propagation of the THz waves outside the interaction volume, has been reported in Refs. [22,23]. Because the noncollinear phase-matching angle between the pump and the THz waves is as large as 65°, this factor has a significant influence on the g_{THz} calculation. In our case, the additional loss factor was estimated to be approximately 30 cm^{-1} [22,23]. Therefore, we included this factor in the calculation as $\alpha_{pr} = 30\,\mathrm{cm}^{-1}$.

The calculated result for the frequency dependence of g_{THz} is represented by the dashed line in Fig. 4(a); this result is in good agreement with the measured g_{THz} around 2.4 THz. Note here that because of α_{pr}, the g_{THz} calculated in this study is smaller than that obtained previously [20]. Below 1.6 THz and above 2.8 THz, however, the experimentally measured g_{THz} was smaller than the theoretical result. This discrepancy is possibly due to the imprecise theoretical calculation because the result of the constant character of $g_{\mathrm{THz}}L_{\mathrm{th}}$ provides evidence that the measured g_{THz} is reliable. On the lower-frequency side, theoretical g_{THz} decreases with increasing α_{pr}. This means that α_{pr} in this study should be larger than 30 cm^{-1} as reported in Refs. [22,23]. On the higher-frequency side, on the other hand, theoretical g_{THz} depends on the constant damping of the A_1 symmetry mode at 7.5 THz in $LiNbO_3$. Further studies are required to determine the α_{pr} and the damping parameters of $LiNbO_3$, and therefore the theoretical calculation needs to be modified in order to be consistent with the experimental result.

Our finding suggests that the performance of SRS-based THz-wave sources can be enhanced by considering $g_{\mathrm{THz}}L_{\mathrm{th}}$. One of the potentialities is output power enhancement by increasing g_{THz}. Because g_{THz} can be increased by a factor of 2 via cryogenic cooling of $LiNbO_3$ to liquid-nitrogen temperature [27], the peak power of the THz-wave output is scalable to MW level. In that case, L should be shortened because of the resultant decrease in L_{th}. Such MW-peak-power monochromatic THz-wave pulses correspond to multicycle electric fields with strengths on the order of MV/cm at the diffraction-limited focus spot. Such a high-strength electric field promises to be a powerful tool for studying diverse THz-wave-induced nonlinear phenomena in a variety of physical systems [1–5,28–31]. Another possibility is tunability widening using $LiNbO_3$ with larger L than that considered in the present study. Because of the decrease in g_{THz} below 0.8 THz and above 3.0 THz, L should be lengthened to exceed L_{th}. Thus, ultrawide tunability from less than 0.5 THz to more than 4 THz is feasible, which would yield a

useful THz-wave source for practical applications, such as high-resolution sensing [13] and nondestructive imagings [32].

In conclusion, we have demonstrated accurate measurement of g_{THz} in $LiNbO_3$ using the surface-coupling configuration. We have experimentally determined the frequency dependence of g_{THz} under SBS suppression. Our approach is applicable not only to $LiNbO_3$, but also to other crystals. This paper, therefore, facilitates the design and performance enhancement of SRS-based ultrabright tabletop THz-wave sources in many laboratories for various applications.

The authors would like to thank Professor H. Ito of RIKEN/Tohoku University and Professor M. Kumano of Tohoku University for fruitful discussions. The authors are also grateful to all members of the Tera-Photonics Research Team. This work was supported, in part, by JSPS KAKENHI Grants No. 15K18079, No. 25220606, and No. 26390106, JST Collaborative Research Based on Industrial Demand, and collaborative research with PHLUXi, Inc. Y. Takida acknowledges support from the RIKEN Special Postdoctoral Researcher Program.

[1] T. Kampfrath, K. Tanaka, and K. Nelson, Nat. Photonics **7**, 680 (2013).
[2] M. Beck, I. Rousseau, M. Klammer, P. Leiderer, M. Mittendorff, S. Winnerl, M. Helm, G. N. Gol'tsman, and J. Demsar, Phys. Rev. Lett. **110**, 267003 (2013).
[3] R. Matsunaga, N. Tsuji, H. Fujita, A. Sugioka, K. Makise, Y. Uzawa, H. Terai, Z. Wang, H. Aoki, and R. Shimano, Science **345**, 1145 (2014).
[4] K. Uchida, H. Hirori, T. Aoki, C. Wolpert, T. Tanaka, K. Tanaka, T. Mochizuki, C. Kim, M. Yoshita, H. Akiyama, L. N. Preiffer, and K. W. West, Appl. Phys. Lett. **107**, 221106 (2015).
[5] T. Kubacka, J. A. Johnson, M. C. Hoffmann, C. Vicario, S. de Jong, P. Beaud, S. Grübel, S.-W. Huang, L. Huber, L. Patthey, Y.-D. Chuang, J. J. Turner, G. L. Dakovski, W.-S. Lee, M. P. Minitti, W. Schlotter, R. G. Moore, C. P. Hauri, S. M. Koohpayeh, V. Scagnoli, G. Ingold, S. L. Johnson, and U. Staub, Science **343**, 1333 (2014).
[6] C. H. Henry and J. J. Hopfield, Phys. Rev. Lett. **15**, 964 (1965).
[7] C. H. Henry and C. G. B. Garrett, Phys. Rev. **171**, 1058 (1968).
[8] S. K. Kurtz and J. A. Giordmaine, Phys. Rev. Lett. **22**, 192 (1969).
[9] J. M. Yarborough, S. S. Sussman, H. E. Purhoff, R. H. Pantell, and B. C. Johnson, Appl. Phys. Lett. **15**, 102 (1969).
[10] M. A. Piestrup, R. N. Fleming, and R. H. Pantell, Appl. Phys. Lett. **26**, 418 (1975).
[11] K. Kawase, M. Sato, T. Taniuchi, and H. Ito, Appl. Phys. Lett. **68**, 2483 (1996).
[12] J. Hebling, A. G. Stepanov, G. Almási, B. Bartel, and J. Kuhl, Appl. Phys. B: Lasers Opt. **78**, 593 (2004).
[13] R. Guo, K. Akiyama, H. Minamide, and H. Ito, Appl. Phys. Lett. **90**, 121127 (2007).
[14] S. Hayashi, K. Nawata, T. Taira, J. Shikata, K. Kawase, and H. Minamide, Sci. Rep. **4**, 5045 (2014).
[15] G. W. Faris, L. E. Jusinski, and A. P. Hickman, J. Opt. Soc. Am. B **10**, 587 (1993).
[16] A. de Bernabé, C. Prieto, and A. de Andrés, J. Appl. Phys. **79**, 143 (1996).
[17] L. Pálfalvi, J. Hebling, J. Kuhl, Á. Péter, and K. Polgar, J. Appl. Phys. **97**, 123505 (2005).
[18] K. Kawase, M. Sato, K. Nakamura, T. Taniuchi, and H. Ito, Appl. Phys. Lett. **71**, 753 (1997).
[19] S. S. Sussman, Microwave Laboratory Tech. Report No. 1851, Stanford University, 1970 (unpublished).
[20] J. Shikata, K. Kawase, K. Karino, T. Taniuchi, and H. Ito, IEEE Trans. Microwave Theory Tech. **48**, 653 (2000).
[21] S. Ushioda, J. D. McMullen, and M. J. Delaney, Phys. Rev. B **8**, 4634 (1973).
[22] U. T. Schwarz and M. Maier, Phys. Rev. B **53**, 5074 (1996).
[23] U. T. Schwarz and M. Maier, Phys. Rev. B **58**, 766 (1998).
[24] T. Ikari, X. Zhang, H. Minamide, and H. Ito, Opt. Express **14**, 1604 (2006).
[25] K. Imai, K. Kawase, H. Minamide, and H. Ito, Opt. Lett. **27**, 2173 (2002).
[26] A. J. Lee and H. M. Pask, Opt. Express **23**, 8687 (2015).
[27] J. Shikata, M. Sato, T. Taniuchi, H. Ito, and K. Kawase, Opt. Lett. **24**, 202 (1999).
[28] P. Gaal, K. Reimann, M. Woerner, T. Elsaesser, R. Hey, and K. H. Ploog, Phys. Rev. Lett. **96**, 187402 (2006).
[29] M. Jewariya, M. Nagai, and K. Tanaka, Phys. Rev. Lett. **105**, 203003 (2010).
[30] F. Junginger, B. Mayer, C. Schmidt, O. Schubert, S. Mährlein, A. Leitenstorfer, R. Huber, and A. Pashkin, Phys. Rev. Lett. **109**, 147403 (2012).
[31] O. Schubert, M. Hohenleutner, F. Langer, B. Urbanek, C. Lange, U. Huttner, D. Golde, T. Meier, M. Kira, S. W. Koch, and R. Huber, Nat. Photonics **8**, 119 (2014).
[32] K. Kawase, Y. Ogawa, Y. Watanabe, and H. Inoue, Opt. Express **11**, 2549 (2003).